Simultaneous electrochemical-electron spin resonance measurements. II. Kinetic measurments using constant current pulse

Ira B. Goldberg, and Allen J. Bard

More About This Article

The permalink http://dx.doi.org/10.1021/j100596a021 provides access to:

- Links to articles and content related to this article
- Copyright permission to reproduce figures and/or text from this article

Simultaneous Electrochemical–Electron Spin Resonance Measurements. II. Kinetic Measurements Using Constant Current Pulse[1]

Ira B. Goldberg*

Science Center, Rockwell International, Thousand Oaks, California 91360

and Allen J. Bard

Chemistry Department, University of Texas at Austin, Austin, Texas 78712   (Received June 18, 1973)

Publication costs assisted by Rockwell International

The application of simultaneous electrochemical–electron spin resonance (seesr) measurements to obtain rate constants of homogeneous reactions involving electrochemically generated radical ion is discussed. Digital simulation methods were used to compute the time dependence of an esr signal during and following a constant current pulse. Reaction mechanisms involving first-order decomposition, radical ion dimerization, and radical–parent dimerization are discussed. Curves from which the rate constants can be obtained are presented.

Introduction

The observation of electrochemically generated radical ions by electron spin resonance (esr) has been used in numerous studies. Various cells and experimental procedures have been described in texts[2] and reviews.[3-5] Radicals can be generated either outside of the esr cavity and placed or flowed into the cavity, or they can be generated directly in the cavity (*intra-muros* or *in-situ* generation).

One of the problems inherent in *in-situ* electrochemical generation is the potential drop through the solution over the length of the working electrode which results in a nonuniform current distribution[6] at the working electrode. This effect results from two requirements of the cell: a small cross-sectional area must be used to minimize microwave power dissipation due to the solution in the cavity and a long working electrode and high current must be used to observe a strong signal. To overcome this problem Goldberg and Bard[1] constructed a flat electrochemical cell for rectangular microwave cavities, which permits simultaneous electrochemical-esr (seesr) experiments. In this cell the ir drop over the length of solution in the cavity is sufficiently small so that the electrochemical parameters could be measured or controlled accurately while the esr signal is recorded. Furthermore, it was demonstrated that when stable radicals are generated by a current pulse, there is a linear rise of esr signal during the pulse, followed by a steady signal, provided the duration of the experiment is limited to 20–30 sec. After this time, convection and reaction between products of the working and auxiliary electrodes begins. The ability to maintain a steady state esr signal indicates that there is no redistribution of electrode products in the seesr cell which has been the case for many *in-situ* cells,[6] and suggests that kinetic measurements can be made using this cell.

Esr measurements of reaction rates of electrolytically generated radicals have involved flow systems or stopped flow systems.[7-9] A cell design somewhat similar to the one used here also required a flow, but in addition required extensive signal averaging.[10] In this case, rate constants could not be determined, but an estimation of the lifetime could be made.

Electrochemical measurements of homogeneous reaction rates of electrogenerated intermediates usually involve a measurement of the current or potential as a function of time. Often electrochemical measurements are coupled with spectroscopic measurements to identify the particular reaction intermediates. Esr has been useful in the identification of paramagnetic intermediates such as radical ions. In cases where more than one intermediate is generated, it is often difficult to distinguish between the rates of reaction of each intermediate from electrochemical measurements especially when the intermediates are electroactive in the same potential region. Using spectroscopic techniques it is sometimes possible to measure the time dependence of signals which can be attributed to each intermediate. Furthermore, esr should show different spectra for adsorbed species at the electrode than for dissolved species. Often secondary intermediates can be formed which also undergo electron transfer and, therefore, contribute to the current. This may be especially significant when electrochemical reversal measurements are used to measure reaction rates, and could lead to erroneous values for the measured rate. This problem can be partially eliminated by spectroscopic measurements.

This paper suggests a current pulse method of measuring the homogeneous kinetic behavior of electrogenerated radical ions, and shows the appropriate "working curves" from which first- and second-order rate constants can be obtained from seesr measurements. A following paper[11] will show the application of this technique in studies of hydrodimerization of activated olefin radical anions. Similar calculations could also be used for spectroelectrochemical measurements.[12]

The following mechanisms are considered. The initial step in each case is the electrochemical generation of a paramagnetic intermediate

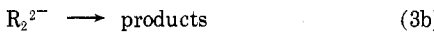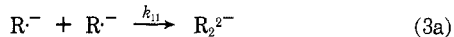$$R + e \rightleftharpoons R^{\cdot -} \qquad (1)$$

All reactions are written for an initial reduction to the radical anion. The parallel case for radical cations will behave in a similar manner. Either of the three following chemical reactions given in eq 2–4 can then take place. The method of digital simulations by finite difference

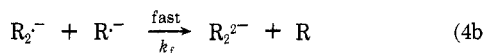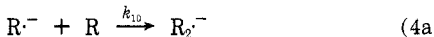equations for a constant current pulse is used to treat the second-order cases.

First-order decomposition

$$R^{-} \xrightarrow{k_1} \text{products} \qquad (2)$$

Radical ion dimerization

$$R^{-} + R^{-} \xrightarrow{k_{11}} R_2^{2-} \qquad (3a)$$

$$R_2^{2-} \longrightarrow \text{products} \qquad (3b)$$

Radical ion–parent dimerization

$$R^{-} + R \xrightarrow{k_{10}} R_2^{-} \qquad (4a)$$

$$R_2^{-} + R^{-} \xrightarrow[k_f]{\text{fast}} R_2^{2-} + R \qquad (4b)$$

$$R_2^{2-} \longrightarrow \text{products} \qquad (4c)$$

Results and Discussion

The method selected for determining homogeneous reaction rates requires the measurement of the esr signal during and following a current pulse time of t_p which is less than or equal to the electrochemical transition time τ of the electrode process as shown by

$$t_p \leqslant \tau = \pi n^2 F^2 A^2 D C_b^2 / 2I^2 \qquad (5)$$

where n, F, A, D, and i have the usual meaning and C_b is the bulk concentration. Maintaining $t_p \leq \tau$ eliminates the problem of less than 100% current efficiency for generation of R^{-} and secondary electrochemical reactions. When the current is stopped, the esr signal will either be constant for stable radical ions or decay. We have chosen to measure the ratio of the esr signal at selected times t_m between $1.1t_p$ and $2.0t_p$ to the signal at t_p. In many cases larger values of t_m would be equally suitable. Typical current–time and signal–time behavior for stable and unstable radical anions is shown in Figure 1. Ratios of the esr signals are used because the absolute signals are not easily related to a specific concentration as in optical measurements. The signal is very dependent upon the exact cell dimensions and positioning in the cavity and also upon the electrode placement in the cavity.

Potential step methods were also considered. Stepping the potential onto the diffusion plateau of an electrochemical wave followed by switching the cell to open circuit[13] could give similar results. Because this procedure always gives the same boundary condition, i.e., the surface concentration of parent material is zero, this is not as useful in providing diagnostic criteria of different mechanisms since several solutions must be studied to completely diagnose kinetic behavior. In comparison a broad range of currents and times can be used with a single solution provided that fresh solution is flowed into the cell after each measurement. One can also consider stepping to potentials on the rising current portion of the electrochemical wave, but this is difficult in this type of cell since there is still a small ir gradient through the solution near the working electrode. If a constant current pulse is used, the double layer charging should be negligible with respect to the faradaic current.

In general for any rate measurement using this cell, the value of t_m should be shorter than 10–20 sec, since convection becomes significant after this time. This coincides with a practical limit of semiinfinite diffusion across
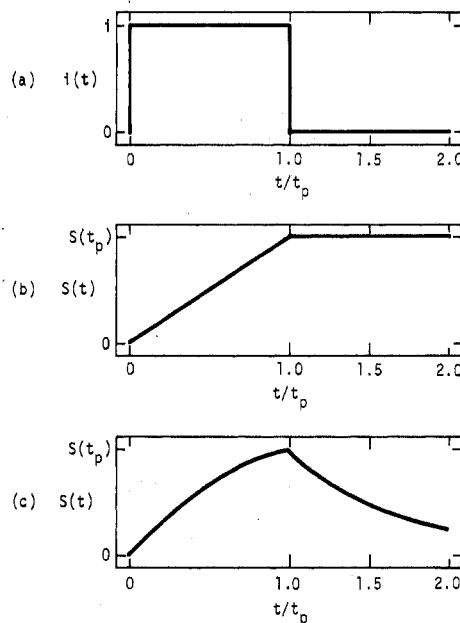

Figure 1. (a) Current–time program for experiment. (b) Signal–time behavior for stable electrogenerated radical. (c) Signal–time behavior for unstable electrogenerated radical.

about 0.3 mm, which is half the thickness of the flat cell, before finite diffusion should be considered. Thus about 10 sec determines an upper limit for the half-life that can be measured by this technique.

Simulations. In the pulse electrolytic method, R^{-} generated at the electrode diffuses into the bulk solution, so that concentrations are nonuniform throughout the cell and the measured esr signal is the integrated signal from the total R^{-} in the cell. In chemical or photochemical methods, the radical species is generated more uniformly throughout the cell, and diffusion is not usually a significant problem. Hence, the mathematical treatment of pulse electrolysis in esr requires solution of the diffusion equations of R^{-} and R with the additional appropriate terms for the chemical reactions for all locations in the cell. This was accomplished by means of digital simulation.

The method of calculation of electrochemical process involving current steps and homogeneous reactions using finite difference methods is similar to that described in detail by Feldberg.[14] In this calculation it is not necessary to compute the potential at each increment during which the current is flowing although this is a good test for convergence of the program, and for whether the transition time has been exceeded. With no controls, it is possible to simulate "negative" concentrations. These calculations were carried out in dimensionless form. The fractional concentration of each species j, in segment k of the simulated diffusion layer $F_j(k)$, was allowed to vary between 0 and 1 where

$$F_j(k) = C_j(k)/C_b \qquad (6)$$

($C_j(k)$ is the true concentration for species j and C_b is the bulk concentration.) Edge effects[15] were not considered, and the electrode was assumed to have unit area.

The variable parameters that were selected were the number of increments M_t during which the current is allowed to flow, the current parameter Z_t, and the reaction rates. The time is determined from the simulation by the

relation

$$t = (m/M_t)t_p \qquad (7)$$

where m is the unit time increment of the simulation. The value of Z_t can be considered as the fraction of the bulk concentration in the solution element adjacent to the electrode which is reduced or oxidized during each time increment of the simulation, and defined according to eq 8

$$Z_t = \frac{1}{FC_bA}\frac{\delta t}{\delta x} \qquad (8)$$

where δt is the time increment t_p/M_t and δx is the thickness of each element of the solution, defined by

$$\delta x = (D\delta t/D_m)^{1/2} \qquad (9)$$

where D is the diffusion coefficient, and D_m is the dimensionless diffusion parameter. The diffusion coefficients of all species were assumed to be equal. The current calculated from the simulation is, therefore

$$i = Z_t nFAC_bD^{1/2}M_t^{1/2}/t_p^{1/2}D_m^{1/2} \qquad (10)$$

First-Order Reactions. The rate parameters can be used in dimensionless form. A first-order reaction during one time increment is given by

$$\delta F_2(k) = -F_2(k)R_1 \qquad (11)$$

where R_1 is the dimensionless kinetic parameter $k_1 \delta t$. A plot of $S(t_m)/S(t_p)$ vs. $k_1 t_p(t_m/t_p - 1)$, as shown in Figure 2, can be used to determine rate constants. Simulations for a first-order reaction are not necessary, and this curve can easily be calculated from

$$\frac{S(t_m)}{S(t_p)} = \exp\left[-k_1 t_p\left(\frac{t_m}{t_p} - 1\right)\right] \qquad (12)$$

where $t_m \geq t_p$. As a test for convergence and accuracy of the digital simulation, calculations were made using different numbers of time increments, M_t, to simulate the current pulse. These results are shown in Table I. Two facts become evident from these results. As expected, as the number of increments is increased, the accuracy of the digital simulation is improved. However, the rate term $k_1 \delta t$ which represents the fraction of R·⁻ lost during each time increment also decreases with an increase in M_t and therefore improves the accuracy of the simulation. It was found that to obtain reasonable accuracy a value of 0.05 or less should be used.

Radical Ion Dimerization. Calculations of the mechanism described in eq 3 were also carried out by digital simulations. No assumption need be made about the rate of eq 3b other than either R_2^{2-} exhibits no esr spectrum or that suitable lines of R⁻ can be found which do not overlap those of R_2^{2-}. Although R_2^{2-} is probably diamagnetic, it could also be a biradical. When electrochemical reversal measurements are used to determine rate constants, it must be assumed that R_2^{2-} does not contribute to the reverse current. In this mechanism the decrease of radicals during one time increment is given by

$$\delta F_2(k) = -R_{11}F_2(k)^2 \qquad (13)$$

where R_{11} is the dimensionless rate parameter, given by

$$R_{11} = 2k_{11}\delta tC_b \qquad (14)$$

A useful curve similar to Figure 2 requires the formulation of parameters that will fit a wide variety of k_{11}, i, and t_p.
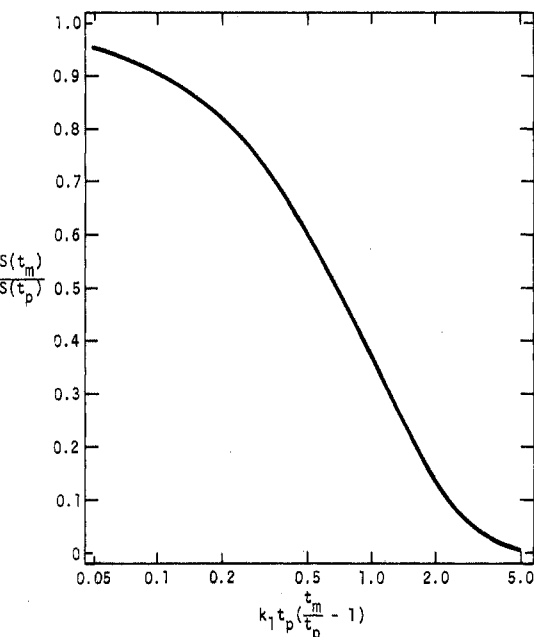
Figure 2. Signal dependence on the rate constant of a first-order decomposition reaction.

TABLE I: Digital Simulation of First-Order Reaction[a]

		$S(t_m)/S(t_p)$			
			$t_m/t_p =$		
M_t	R_1	1.10	1.20	1.50	2.00
25	0.08		0.6591		0.1244
50	0.04	0.8154	0.6648	0.3604	0.1299
100	0.02	0.8171	0.6676	0.3642	0.1326
200	0.01	0.8179	0.6690	0.3660	0.1340
500	0.004	0.8184	0.6698	0.3675	0.1348
Theoretical[b]		0.8187	0.6703	0.3680	0.1353

[a] $k_1 t_p = 2.00$. [b] Calculated from eq 12.

To find these parameters we assume the limiting condition that the concentration of R·⁻ generated is uniform, so that the average concentration would be of the form $it_p^{1/2}/nFAD^{1/2}$.

The dimensionless parameter for this system which is analogous to that of the usual second-order parameter $k_{11}tC_R^-$ then becomes

$$Y_{11} = ik_{11}t_p^{3/2}/nFAD^{1/2} \qquad (15)$$

The dimensional parameters can be related to the dimensionless parameters described in eq 6-9 and Y_{11} can also be shown to be related to real parameters through

$$\frac{Y_{11}}{Z_t}\frac{D_m^{1/2}}{M_t^{1/2}} = k_{11}t_pC_b \qquad (16)$$

Values of $S(t_m)/S(t_p)$ for various values of Y_{11} are given in Table II, and these data are shown plotted in Figure 3. A suitable curve can be selected for each set of data. The most precise determination of k appears to be in the region where $S(t_m)/S(t_p)$ is between 0.3 and 0.8.

Radical-Ion Parent Dimerization. Theoretical signal-time curves obtained for the mechanism described in eq 4 were considerably more difficult to normalize to appropriate parameters than either of the other mechanisms. Several assumptions must be made here. In general, intermediates of the form R_2^- react with R·⁻ as in eq 4b are also

TABLE II: Values of the Ratio $S(t_m)/S(t_p)$ with Variation of Current, Rate Constant, and Pulse Time for Radical Ion Dimerization

$\dfrac{ikt_p{}^{3/2}}{nFAD^{1/2}}$	$t_m/t_p =$	$S(t_m)/S(t_p)$				$\dfrac{ikt_p{}^{3/2}}{nFAD^{1/2}}$	$t_m/t_p =$	$S(t_m)/S(t_p)$			
		1.10	1.25	1.50	2.00			1.10	1.25	1.50	2.00
0		1.000	1.000	1.000	1.000	14.00		0.739	0.569	0.434	0.314
0.15		0.984	0.964	0.937	0.895	30.00		0.662	0.485	0.358	0.252
0.40		0.963	0.919	0.963	0.784	75.00		0.564	0.392	0.280	0.192
0.70		0.943	0.879	0.802	0.701	200.00		0.464	0.308	0.214	0.144
1.30		0.914	0.825	0.724	0.605	750.00		0.354	0.226	0.154	0.102
2.50		0.876	0.759	0.639	0.509	3000.0		0.306	0.192	0.130	0.086
6.00		0.812	0.664	0.530	0.400						

electroactive. If the rate of this reaction is very fast, i.e., much faster than in eq 4a, then the amount of $R_2\cdot{}^-$ at the electrode is small and can be neglected. It is also likely that $R_2\cdot{}^-$ is paramagnetic. Based on the previous assumption that reaction 4b is fast, however; there will be no contribution to the esr spectrum from this material. The same consideration of $R_2{}^{2-}$ described in the previous section also applies.

The rate equations for this mechanism are

$$d[R\cdot{}^-]/dt = -k_{10}[R\cdot{}^-][R] - k_f[R\cdot{}^-][R_2\cdot{}^-] \quad (17a)$$

$$d[R]/dt = -k_{10}[R\cdot{}^-][R] + k_f[R\cdot{}^-][R_2\cdot{}^-] \quad (17b)$$

Because the rate of eq 4b is fast, a steady-state approximation can be made for species R, so that setting $d[R]/dt = 0$

$$d[R\cdot{}^-]/dt = -2K_{10}[R\cdot{}^-][R] \quad (18)$$

In terms of the digital simulation this becomes

$$\delta F_2(k) = -2k_{10}C_b\delta t F_1(k)F_2(k) = R_{10}F_1(k)F_2(k) \quad (19)$$

where $F_2(k)$ represents the relative concentration of $R\cdot{}^-$, and $F_1(k)$ represents the relative concentration of R. The amount of R is essentially unchanged during the chemical reaction following the cessation of the current pulse. In order to obtain a suitable dimensionless ordinate to plot the signal dependence, consider the limiting conditions that a small amount of $R\cdot{}^-$ is generated uniformly throughout the solution. In this case the reaction rate becomes pseudo-first order so that

$$d[R\cdot{}^-]/dt \longrightarrow -2k_{10}(C_b - \overline{[R\cdot{}^-]})[R\cdot{}^-] \quad (20)$$

where $\overline{[R\cdot{}^-]}$ can represent a weighted average concentration of $R\cdot{}^-$ in the diffusion layer. As suggested earlier, this value should have the form $Pit_p{}^{1/2}/nFAD^{1/2}$ which has units of concentration, and P is a dimensionless constant. Equation 20 suggests that a suitable parameter could therefore be

$$Y_{10} = k_{10}t_p\left(C_b - P\frac{it_p{}^{1/2}}{nFAD^{1/2}}\right) \quad (21)$$

where P depends upon t_m/t_p, i.e., P should decrease as the diffusion layer size increases. Digital simulations confirm this behavior. The best values of P were found to be 0.73 when $t_m/t_p = 1.1$, 0.67 when $t_m/t_p = 1.2$, 0.55 when $t_m/t_p = 1.5$, and 0.45 when $t_m/t_p = 2.0$. For eq 21 to be valid, C_b must always be larger than $Pit_p{}^{1/2}/nFAD^{1/2}$. The case where t_p is equal to the electrochemical transition time (eq 5) determines the upper limit for P to be 1.128. In the case where $t_p \ll t_m$, P should approach zero, and the reaction would appear pseudo-first order. This result is confirmed by digital simulations.

Ratios of $S(t_m)/S(t_p)$ for various values of Y_{10} at the optimum values of P are shown in Table III and plotted in

TABLE III: Values of the Ratio $S(t_m)/S(t_p)$ with Variation of Current, Rate Constant, and Pulse Time for Radical–Ion Parent Dimerization

| Y_{10} ($P = 0.45$)	$S(2t_p)/S(t_p)$	Y_{10} ($P = 0.55$)	$S(1.5t_p)/S(t_p)$	Y_{10} ($P = 0.67$)	$S(1.2t_p)/S(t_p)$
0.000	1.000	0.000	1.000	0.000	1.000
0.056	0.894	0.105	0.895	0.266	0.892
0.115	0.791	0.239	0.785	0.600	0.779
0.178	0.700	0.345	0.704	0.870	0.700
0.227	0.635	0.435	0.639	1.166	0.622
0.345	0.498	0.690	0.497	1.628	0.513
0.443	0.410	0.940	0.390	2.28	0.400
0.575	0.316	1.313	0.268	2.80	0.329
0.863	0.180	1.725	0.176	3.99	0.200
1.163	0.099	2.506	0.095	5.50	0.106
2.100	0.012	4.350	0.014	10.58	0.015
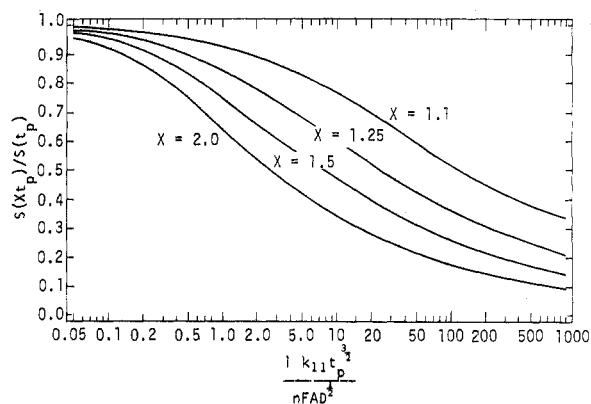
Figure 3. Signal dependence for the second-order radical ion dimerization reaction at different values of t_m/t_p ($X = t_m/t_p$).

Figure 4. Calculated values of $S(t_m)/S(t_p)$ for the same Y_{10} with different values of Z_t (eq 8), M_{tp}, and k_{10} agree to within 0.003 units. Thus, although eq 21 may not be an exact description of the behavior of this sysem, it appears accurate enough for the diagnosis of mechanism and the estimation of rate constants. After the best values of P were chosen, it was found that the collected data could be plotted on same axis (Figure 5) by multiplying Y_{10} by $(t_m/t_p - 1)$. Calculated points for different values of t_m/t_p are shown to provide comparison of results. Figure 5 can also be used for the determination of rate constants. To make full use of this diagram, however, P must be determined as a function of t_m/t_p.

Conclusion

We expect that the technique of simultaneous current pulse and esr signal–time measurement can be used to elucidate a wide variety of reaction mechanisms. These examples, mainly drawn from possible dimerization
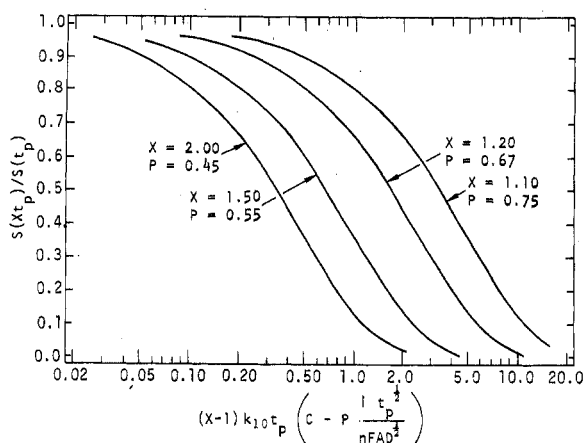
Figure 4. Signal dependence for the second-order radical–ion parent reaction at different values of t_m/t_p ($X = t_m/t_p$).

Figure 5. Signal dependence for the second-order radical–ion parent reaction at different values of t_m/t_p: $t_m/t_p = 1.1$, $\bigcirc$; $t_m/t_p = 1.2$, $\triangle$; $t_m/t_p = 1.5$, $\blacktriangle$; $t_m/t_p = 2.0$, $\bullet$.

routes,[16] serve to illustrate and approach to the determination measurement of rate constants and reaction pathways. The application of this treatment is demonstrated in a companion paper.[11] Esr offers the advantage of being able to monitor individual electrogenerated radical ions in a mixture, and is not as sensitive to contributions of secondary electroactive intermediates.

Acknowledgments. The authors thank Dr. C. S. Burton for helpful discussions. The support of the National Science Foundation (GP-6688X) and the Robert A. Welch Foundation is gratefully acknowledged.

Appendix

Dimensional Variables

A = electrode area, cm²
C_b = bulk concentration, mol/cm³
D = diffusion coefficient, cm²/sec
F = Faraday, 96,500 C/mol
i = current, A
k_1 = first-order rate constant, sec⁻¹
k_{10} = radical–ion parent dimerization, cm³ mol⁻¹ sec⁻¹
k_{11} = radical ion dimerization, cm³ mol⁻¹ sec⁻¹
n = number of electrons transferred
t_m = time of measurement of esr signal, sec
t_p = duration of current pulse, sec
x = distance normal to electrode
δ = increment
τ = electrochemical transition time

Indices

k = index of length perpendicular to electrode
j = species $j = 1$, R; $j = 2$, R·⁻
m = index of time

Variables

D_m = diffusion parameter used in finite difference methods
$F_j(k)$ = fractional concentration of species j at center of ith increment
M_t = number of time increments
R_1 = rate term used in simulation for k_1
R_{10} = rate term used in simulation for k_{10}
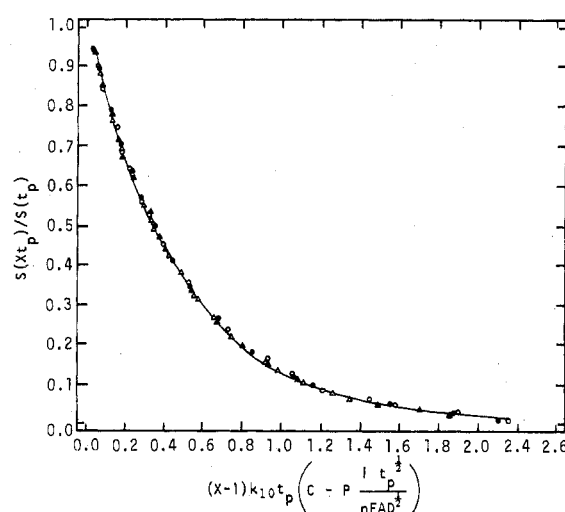R_{11} = rate term used in simulation for k_{11}
Z_t = current

Supplementary Material Available. More complete tables of $S(t_m)/S(t_p)$ for $t_m/t_p = 2.00$, 1.50, 1.20, and 1.10[17] for both dimerization mechanisms presented will appear following these pages in the microfilm edition of this volume of the journal. Photocopies of the supplementary material from this paper only or microfiche (105 × 148 mm, 24× reduction, negatives) containing all of the supplementary material for the papers in this issue may be obtained from the Journals Department, American Chemical Society, 1155 Sixteenth St., N.W., Washington, D. C. Remit check or money order for $3.00 for photocopy or $2.00 for microfiche referring to code number JPC-74-290.

References and Notes

(1) Part I, I. B. Goldberg and A. J. Bard, *J. Phys. Chem.*, **75**, 3281 (1971).
(2) C. P. Poole, "Electron Spin Resonance," Interscience, New York, N. Y., 1967, pp 624–633; R. S. Alger, "Electron Paramagnetic Resonance," Interscience, New York, N. Y., 1968, pp 267–272.
(3) R. N. Adams, *J. Electroanal. Chem.*, **8**, 151 (1964).
(4) I. B. Goldberg and A. J. Bard in "Magnetic Resonance in Chemistry and Biology," Marcel Dekker, New York, N. Y., in press.
(5) B. Kastening, *Chem. Ing. Tech.*, **42**, 190 (1970).
(6) I. B. Goldberg, A. J. Bard, and S. W. Feldberg, *J. Phys. Chem.*, **76**, 2550 (1972).
(7) R. Koopmann and H. Gerischer, *Ber. Bunsenges. Phys. Chem.*, **70**, 118 (1966); R. Koopmann, *ibid.*, **70**, 121 (1966); R. Koopmann and H. Gerischer, *ibid.*, **70**, 127 (1966).
(8) K. Umemoto, *Bull. Chem. Soc. Jap.*, **40**, 1058 (1967).
(9) B. Kastining and S. Vavricka, *Ber. Bunsenges. Phys. Chem.*, **72**, 27 (1968).
(10) R. Hirasawa, T. Mukaibo, H. Hasegawa, N. Odan, and T. Maruyama, *J. Phys. Chem.*, **72**, 2541 (1968).
(11) I. B. Goldberg, R. Hirasawa, D. W. Boyd, and A. J. Bard, *J. Phys. Chem.*, **78**, 295 (1974).
(12) M. Petek, T. E. Neal, R. L. McNeely, R. W. Murray, *Anal. Chem.*, **45**, 32 (1973); R. W. Murray, W. R. Heineman, and G. W. O'Dom, *Anal. Chem.*, **39**, 1666 (1967).
(13) S. Bruckenstein and B. Miller, *J. Electrochem. Soc.*, **117**, 1040 (1970).
(14) S. W. Feldberg, *Electroanal. Chem.*, **3**, 199 (1969).
(15) J. B. Flanagan and L. S. Marcoux, *J. Phys. Chem.*, **77**, 1051 (1973).
(16) W. V. Childs, J. T. Maloy, C. P. Keszthelyi, and A. J. Bard, *J. Electrochem. Soc.*, **118**, 874 (1971); V. J. Puglisi and A. J. Bard, *ibid.*, **119**, 829 (1972).
(17) Copies of these tables are available from the authors. Copies will be supplied by the authors in responses to reprint requests.